A Planning Method for Synchronous Condensers in Weak Grids Using Semi-definite Optimization

Sajjad Hadavi, *Student Member, IEEE,* James Saunderson, *Member, IEEE,*
Ali Mehrizi-Sani, *Senior Member, IEEE*, Behrooz Bahrani, *Senior Member, IEEE*

***Abstract*—Synchronous Condensers (SynCons) offer voltage regulation, inertia, and fault current contribution to solve the challenges of voltage and frequency instability introduced by the high penetration of renewable energy resources (RERs). However, the cost of installation and operation of a SynCon is noticeable. Furthermore, the SynCons installation can take more than a year, which means the number, size, and placement of the SynCons must be selected optimally. This paper proposes a method to formulate the optimal sizing and allocation of the SynCons via mixed-integer convex optimization. The optimization procedure aims to minimize the cost of SynCons installation, maintenance, and operation while maintaining a certain Short Circuit Ratio (SCR) at points of connection (PoCs). To ensure the SCR at the PoCs is greater than a certain threshold, the SCRs are formulated as constraints in the proposed optimization procedure. The modified IEEE 39-bus system is used to evaluate the proposed optimization method. The performance of the system with optimal SynCons is verified by electromagnetic transient time-domain simulation using PSCAD/EMTDC software. The simulation results show that the system with the optimal installation of SynCons performs better than the system without the SynCons or with a non-optimal installation of SynCons. With the optimized system, all renewable energy resources are stable after contingencies.**

***Index Terms*—Convex optimization, Synchronous condenser, Weak grid.**

NOMENCLATURE

a_k	Desired Minimum Value Short Circuit Ratio
b_k	Optimization Constraint $=\frac{1}{a_k}$
c_i	Coefficient of the Installation, Operation, and Maintenance Cost of ith SynCons
EMT	Electromagnetic Transient
FRT	Fault Ride-Through
GA	Genetic Algorithm
LMI	Linear Matrix Inequality
MFRT	Multiple Fault Ride-Through
MSE	Mean Square Error
N	Number of Available SynCons
NER	Australian National Electricity Rules
PoC	Point of Connection
RER	Renewable Energy Resources
S_{base}	Base Apparent Power of a System
s_i	Indicate whether a SynCon will be installed at ith bus
$\overline{S_{\text{syn}_i}}$	Maximum Available Capacity of ith SynCon
S_{syn_i}	ith SynCon Capacity
$\underline{S_{\text{syn}_i}}$	Minimum Available Capacity of ith SynCon
$\overline{\text{SCR}}^i$	Short Circuit Ratio
SDP	Semi-Definite Program
SSO	Sub-Synchronous Oscillations
stdev	Standard Deviation
V	Number of Buses in a System
W_{bus}	Real Symmetric Matrix, $=j[Y_{\text{bus}}]$
$\text{diag}(W)$	Diagonal Matrix with Diagonal Elements Given by the Vector W
$X_{\text{sc}^k_{pu}}$	Impedance of the kth SynCon in pu
Y_{bus}	Admittance Matrix of a System
y_{ij}	Admittance Between Buses i and j
y_i	Self-Admittance at the ith Bus
Z_{eq}	Equivalent Impedance of the System from the PoC
Z_{bus}	Impedance Matrix of a System

I. INTRODUCTION

DUE to environmental challenges and global climate change, fossil fuel-based generators are being replaced by Renewable Energy Resources (RERs). The majority of RERs are connected to power systems with power electronic converters, which cannot provide the same inertia as fossil fuel-based generators. The high penetration of the RERs and the retirement of old fossil fuel-based generators decrease inertia in power systems [1]–[3]. Moreover, most RERs are placed in rural areas and are connected to power systems via long transmission lines. A long transmission line means a large impedance, which decreases the Short Circuit Ratio (SCR) in a power system [4]–[6].

The reduction of the SCR to values less than 3 and the low inertia in a power system create weak grids [7], which can lead to new challenges, such as Sub-Synchronous Oscillations (SSOs) [8]–[12]. In recent years, there has been an increasing interest in weak grid integration and operation enhancement of RERs [13]–[16]. One possible solution for overcoming the shortcomings caused by high penetration of RERs in weak grids and enhancing system strength is Synchronous Condensers (SynCons) [17]–[21].

SynCon is a synchronous machine without a prime-mover, which is used in power systems to provide inertia, regulate voltage with absorption or injection of reactive power, and increase system strength [22], [23]. Furthermore, SynCons can contribute to fault current. However, one of the main obstacles in utilizing SynCons is their capital and operational cost, which highlights the importance of their optimal sizing and allocation [18], [24]–[29]. In [24], an optimal location of SynCons is obtained based on each SynCon's reactive power contribution and its influence on power flow and voltage stability. However, the SynCon installation cost, SCR, and RERs penetration effects are not considered in this method. The impact of SynCons on SCR is investigated in [25], which proposes a methodology

to improve the SCR and the frequency response by utilizing retired synchronous machines as SynCons. However, the post-retirement utilization of synchronous machines only impacts their installation cost, but operation and maintenance costs are neglected. In [26], a mixed-integer dynamic optimization method for allocation of required reactive power in a large-scale power system with wind generation is proposed. However, the proposed method is computationally complex and does not consider the impact of SynCons on the system's SCR and cost.

There are a few studies that have investigated the impact of SynCons on the SCR with consideration of their cost based on meta-heuristic optimization methods. In [27], the objective function is to minimize SynCons cost while maintaining a certain SCR at various buses, but the number of SynCons in the system is not optimal; the optimization procedure is based on meta-heuristic algorithms, such as the Genetic Algorithm (GA), which cannot guarantee the global optimality of the results; and there are no tests to check compliance with standards and grid codes. In [28], a method to determine optimal sizing and allocation of SynCons to enhance SCR at the Point of Connection (PoC) of a wind farm considering the long-term economical impact of SynCon is proposed. However, as in previous studies, the GA is used, which cannot guarantee global optimality. In [29], the optimal location of SynCons is obtained based on heuristic algorithm to minimize a total cost of synchronous condenser installations in a hypothetical future a power system with penetration of RERs and the POCs SCR are strengthened. However, similar the previous studies, the heuristic algorithm cannot guarantee global optimality. In [18] a multi-objective optimization method is proposed to find the optimal number, size, and location of SynCons, while the cost and voltage deviation are minimized. Different meta-heuristic methods are applied to reduce the impact of the local optimization results. However, again, the proposed optimization method cannot guarantee global optimality.

In this paper, under appropriate modelling assumptions, SynCons optimal allocation, sizing, and number in a system with high penetration of RERs is formulated as a mixed-integer convex optimization problem. The proposed optimization method improves the strength and stability in a large power system with high penetration of RERs. The proposed optimization method maintains SCR above desired values for all PoCs, while costs of investment, operation, and maintenance are minimized. The proposed method can be used both when RERs are installed or comissioned to be installed to a power system. In contrast to the existing approaches, the proposed convex optimization approach, when combined with a branch-and-bound scheme, does guarantee global optimality. The results performance are evaluated with Electromagnetic Transient (EMT) time-domain simulation in PSCAD/EMTDC.

The rest of the paper is organized as follows. In Section II, the existing optimization methods for optimally utlizing SynCons and the proposed optimization procedure are presented in. Next, in Section III, the proposed optimization method is implemented in a modified IEEE 39-bus power system to size and allocate SynCons optimally, and the results are evaluated in PSCAD/EMTDC. Finally, Section IV explains the paper conclusions.

II. Optimal Sizing and Allocation of SynCons

In this section, a convex optimization method to perform optimal sizing and allocation of SynCons is proposed. First, a classification for weak and low-inertia grid definition is proposed, then an approach to formulate optimal sizing based on fixed SynCon locations is introduced, and finally, the optimal allocation is added to the formulation.

A. Weak Grid Definition and SynCons Impact

In this paper, for the integration of RERs into a power system, the SCR is used as an index for weak grid classification. A grid with an SCR of less than three is defined as a weak grid, and a grid with an SCR less than two is defined as a very weak grid. In this paper, the SCR at the PoC is calculated as:

$$\mathrm{SCR} = \frac{1}{|Z_{\mathrm{eq}}|}, \tag{1}$$

where Z_{eq} is the equivalent impedance of the grid as seen from the PoC, which is calculated from the admittance matrix. The admittance matrix Y_{bus} is a $|V| \times |V|$ matrix, where $|V|$ is the number of buses in the grid. The (i, j) element of Y_{bus} is

$$[Y_{\mathrm{bus}}]_{i,j} = \begin{cases} y_i + \sum\limits_{n \neq i,\ n \in V} y_{in}, & \text{if } i = j \\ -y_{ij}, & \text{if } i \neq j, \end{cases} \tag{2}$$

where y_i is the self-admittance at the ith bus, and y_{ij} is the admittance between buses i and j. The impedance matrix Z_{bus} for the grid is the inverse of Y_{bus}. The equivalent impedance for each PoC is called $[Z_{\mathrm{eq}}]$ and defined as

$$[Z_{\mathrm{eq}}]_i = [Z_{\mathrm{bus}}]_{ii}, \tag{3}$$

the ith diagonal element of the impedance matrix. Generally, to study the impact of a SynCon on the SCR, the SynCon is modeled as a current source and a parallel impedance as shown in Fig. 2. Installing a SynCon with reactance X_{sc} at bus i causes the diagonal values in the admittance matrix to change as

$$[Y_{\mathrm{bus}}^{\mathrm{new}}]_{ii} = [Y_{\mathrm{bus}}^{\mathrm{old}}]_{ii} + \frac{1}{jX_{\mathrm{sc}}}, \tag{4}$$

but it does not change the off-diagonal entries of the admittance matrix. Therefore, Z_{eq} changes with SynCons installation.

Using meta-heuristic optimization algorithms [18] to solve this optimal sizing and allocation problem for SynCons does not guarantee that optimal solutions can be found. In this paper, in contrast, it is shown how this problem can be reformulated as a convex optimization problem to provide global optimality using commonly available software. Since the X/R ratio is high in a high-voltage power system, transmission lines are assumed to be purely inductive. Since Y_{bus} is purely inductive, it is convenient to define the real symmetric matrix $W_{\mathrm{bus}}{=}j[Y_{\mathrm{bus}}]$, a notation used in the rest of the paper. Since the matrix Y_{bus} is invertible in a power system with non-transformer zero-impedance loops [30], [31], W_{bus} is also invertible. Since W_{bus} is diagonally dominant (DD), it follows

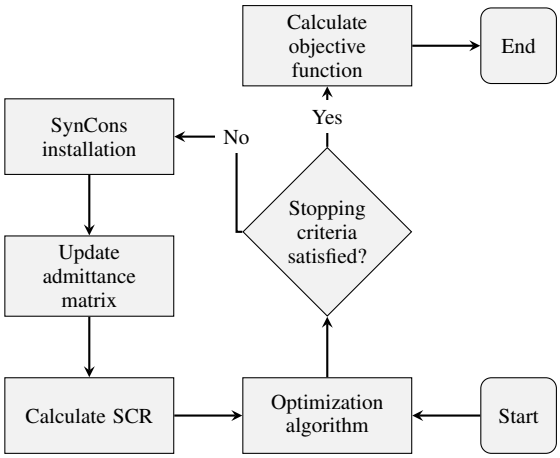

Fig. 1. Flowchart of existing optimization procedures.

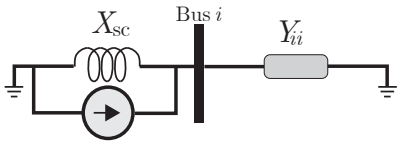

Fig. 2. SynCon impedance model.

from the Gershgorin circle theorem [32] that W_{bus} is positive semi-definite. Since W_{bus} is both invertible and positive semi-definite, it is, in fact, strictly positive definite.

B. Preliminaries on Semi-Definite Programming

A semi-definite program (SDP) is a type of convex optimization problem of the form

$$\min_{x} \quad \sum_{i=1}^{n} d_i x_i \tag{5a}$$

$$\text{s.t.} \quad A_0 + \sum_{i=1}^{n} A_i x_i \succeq 0, \tag{5b}$$

$$Bx = C, \tag{5c}$$

where x is a decision variable of size n, d is a fixed vector with a size equal to n, B and C are fixed matrices, and A_is are fixed symmetric matrices. Here and throughout, the notation $A \succeq 0$ means that the symmetric matrix A is positive semi-definite. As such, an SDP involves minimizing a linear objective function subject to linear equality constraints (5c) and linear matrix inequality (LMI) constraints (5b). Semi-definite optimization problems can be solved efficiently to global optimality using off-the-shelf software (such as the commercial solver MOSEK [33]).

C. Optimal Sizing with Fixed Locations

Suppose the locations of the SynCons are fixed, and the aim is to reduce the installation, operation, and maintenance costs of the SynCons while maintaining the SCR for all PoCs above the desired values. The decision variables are the SynCon capacities, denoted S_{syn_i} for $i \in V$. The objective function is

$$\min_{S_{\text{syn}}} \sum_{i \in V} c_i S_{\text{syn}_i}, \tag{6}$$

where c_i is the cost coefficient of the installation, operation, and maintenance cost of SynCons. The constraint is

$$\text{SCR}_k \geq a_k \quad \text{for } k \in V, \tag{7}$$

where SCR_k is the kth PoC SCR, and a_k is its desired minimum value. Define $W_{\text{bus}}^{\text{new}} = jY_{\text{bus}}^{\text{new}}$, and note that $W_{\text{bus}}^{\text{new}} = W_{\text{bus}} + \text{diag}(W)$ where $\text{diag}(W)$ is a diagonal matrix with diagonal elements given by the vector W. The entries of this vector are obtained by rescaling the SynCon capacity and system base MVA as follows:

$$W_k = \frac{S_{\text{syn}_k}}{X_{\text{sc}_{pu}^k} \times S_{\text{base}}} \quad \text{for } k \in V, \tag{8}$$

where S_{syn_k} is the capacity of the kth SynCon, $X_{\text{sc}_{pu}^k}$ is the impedance of the kth SynCon in pu, and S_{base} is the base apparent power of the system. Note that $\text{diag}(W)$ is linear in the decision variable S_{syn}. By combining (1) with (4) and (7) in one equation, the SCR constraint can be expressed as

$$\frac{1}{[W_{\text{bus}}^{\text{new}}]_{kk}^{-1}} \geq a_k. \tag{9}$$

Since W_{bus} is strictly positive definite and $\text{diag}(W)$ is positive semi-definite, the left-hand side of (9) is strictly positive. Therefore, (9) can be written as

$$[W_{\text{bus}}^{\text{new}}]_{kk}^{-1} \leq b_k, \tag{10}$$

where $b_k = \frac{1}{a_k}$ for the kth PoC.

There are upper and lower bounds on the capacity of the SynCons, which are formulated in one equation with the location of the SynCons. Let $s_i \in \{0, 1\}$ indicate whether a SynCon will be installed at bus i. The capacity constraints are then

$$s_i \underline{S_{\text{syn}_i}} \leqslant S_{\text{syn}_i} \leqslant s_i \overline{S_{\text{syn}_i}} \quad \text{for } i \in V, \tag{11}$$

where $\underline{S_{\text{syn}_i}}$ and $\overline{S_{\text{syn}_i}}$ are the minimum and maximum available capacity of ith SynCon. Note that if $s_i = 0$, indicating that a SynCon is not installed at bus i, the constraint (11) is equivalent to $S_{\text{syn}_i} = 0$.

To formulate the the optimization problem defined by (6) to (11) as an SDP, an LMI-based reformulation of the constraint (10) is used. This reformulation appears as (12b) and (12c), below, and follows from Lemma 1 in Appendix A. A justification of its correctness is also given in Appendix A.

Overall, then, the optimization problem defined by (6) to (11) can be written as a semi-definite program in the decision variables S_{syn_i} (a vector of length $|V|$) and T (a symmetric $|V| \times |V|$ matrix) as follows

$$\min_{S_{\text{syn}}, T} \quad \sum_{i \in V} c_i S_{\text{syn}_i}, \tag{12a}$$

$$\text{s.t.} \quad \begin{bmatrix} T & I \\ I & \text{diag}(W) + W_{\text{bus}} \end{bmatrix} \succeq 0, \tag{12b}$$

$$T_{ii} \leqslant b_i \ \text{ for } i \in V, \tag{12c}$$

$$W_i = S_{\mathrm{syn}_i}/(X^i_{\mathrm{sc}_{pu}} S_{\mathrm{base}}) \quad \text{for } i \in V, \tag{12d}$$

$$s_i \underline{S_{\mathrm{syn}_i}} \leqslant S_{\mathrm{syn}_i} \leqslant s_i \overline{S_{\mathrm{syn}_i}} \quad \text{for } i \in V. \tag{12e}$$

(Here and throughout, I denotes the identity matrix of appropriate dimensions.) Strictly speaking, W is also a decision variable; however, it can clearly be rewritten in terms of S_{syn} and eliminated from the formulation using (12d). It is included in the formulation above only to simplify the notation.

D. Optimal Sizing and Allocation

In the previous section, the vector s is fixed. To simultaneously optimize over SynCon locations and sizes, s_i is allowed to be a binary decision variable. If at most N SynCons should be installed, the constraint

$$s_i \in \{0,1\} \quad \text{for } i \in V \ \text{ and } \ \sum_{i \in V} s_i \leq N, \tag{13}$$

is added to (12) to model the problem of optimal sizing and allocation of SynCons. However, adding this constraint turns the problem into a mixed-integer SDP due to the binary decision variables. This can be solved to global optimality using a branch-and-bound scheme, where each sub-problem is an SDP. In this paper, the branch-and-bond method is used to solve the exact mixed-integer SDP.

III. Performance Evaluation

In this section, the performance of the proposed optimization algorithm is validated based on the tests recommended by the Australian National Electricity Rules (NER) [34]. The proposed optimization is implemented in a large weak and low-inertia grid with high penetration of renewable energy. The system with the optimized location and size of SynCons is modeled in the time-domain simulation environment, PSCAD/EMTDC.

A. Study System Description

The modified IEEE 39-bus system with three RERs (two wind farms and one solar farm) as shown in Fig. 3 is used as the testbed described in [18]. The nominal powers of the added RERs are 200 MW (bus 29), 500 MW (bus 32), and 200 MW (bus 38). IEEE 39-bus system is modified to have an SCR less than 3 at all PoCs to ensure that the system is weak.

B. Optimization Results

The optimization problem with the combination of (12) and (13) is formulated using YALMIP [35] and solved using MOSEK [33]. The optimization problem has 858 constraints, 196 scalar variables, two matrix variables, and 39 binary variables. $\underline{S_{\mathrm{syn}_i}}$, $\overline{S_{\mathrm{syn}_i}}$, and N are 10 MVA, 200 MVA, and 5, respectively. The YALMIP calculation time and the MOSEK solver time are 5.04723 s and 11.7826 s, respectively, in a PC with 16 GB RAM and Intel Core i7 CPU with 1.7 GHz. Also, the number of sub-problems for the branch-and-bound method in worse-case scenario is 2^V. However, in this study, the branch-and-bound method is solved with the sub-problems

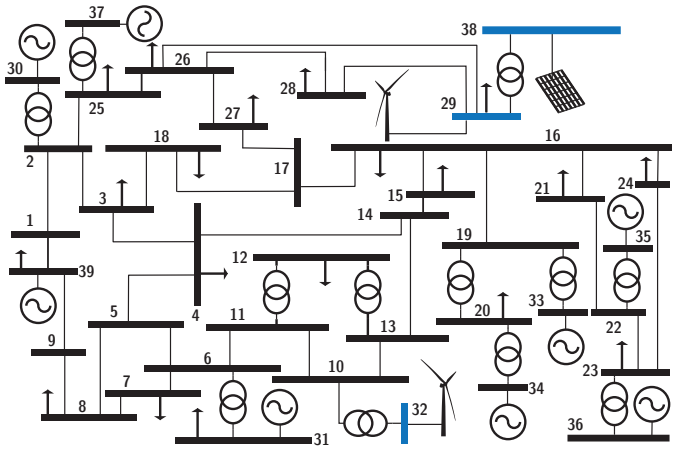

Fig. 3. The configuration of modified IEEE 39-bus System.

TABLE I
Optimization Results

Bus Number	10	29	32	38
Size of SynCon (MVA)	13	16	25	42

TABLE II
Compared Optimization Result For the Augmented IEEE 39-Bus

Optimization Method	**Size (MVA)**	**Cost (M$)**	**minSCR**
SDP	96	3.84	3.08
GA	184	7.44	3.09
Bat	188	7.52	3
HSS	186	7.44	3.03

equal to 23. Therefore, the proposed optimization method is fast and practical in the planning of power systems. The optimization results are given in Table I. The optimized sizes of SynCons are significantly less than the sizes obtained via the meta-heuristic optimization methods used for an identical system in [18]. In [18], the total size for SynCons is 184 MVA, compared with 96 MVA in the proposed optimization method. The optimization results are rounded up to integer values and used in the next section to validate the optimal sizing and allocation of SynCons in the time-domain simulation. The optimization results are compared with the meta-heuristic algorithms and listed in Table II. As given in Table II, with the SDP method, the cost is reduced significantly compared to the meta-heuristic optimization methods.

C. Time-Domain Simulation Verification

PSCAD/EMTDC does the Time-domain simulation to evaluate the optimized results in this paper. Therefore, the modified IEEE 39-bus is modeled in PSCAD/EMTDC. Generic models for a solar farm and a Type IV wind turbine are used. The SynCons exciter is considered an AC1A model [36].

The contingencies applied to the modified IEEE 39-bus system are as follows.

- Fault Ride-Through (FRT) Test: In this contingency, a three-phase fault is applied at all RERs' PoCs at t=9.7 s

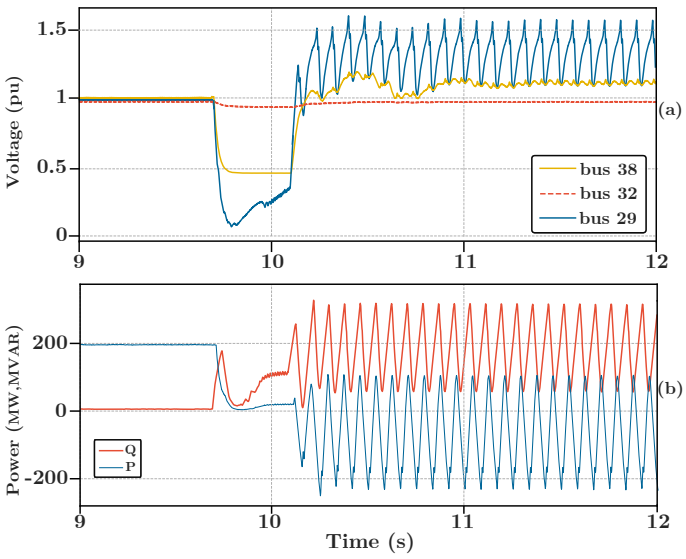

Fig. 4. Time-domain simulation results in the system with no SynCon installation when FRT with the duration of 430 ms happens at bus 29 at t=9.7 s: (a) PoC voltages and (b) reactive and active power of the wind farm connected to bus 29.

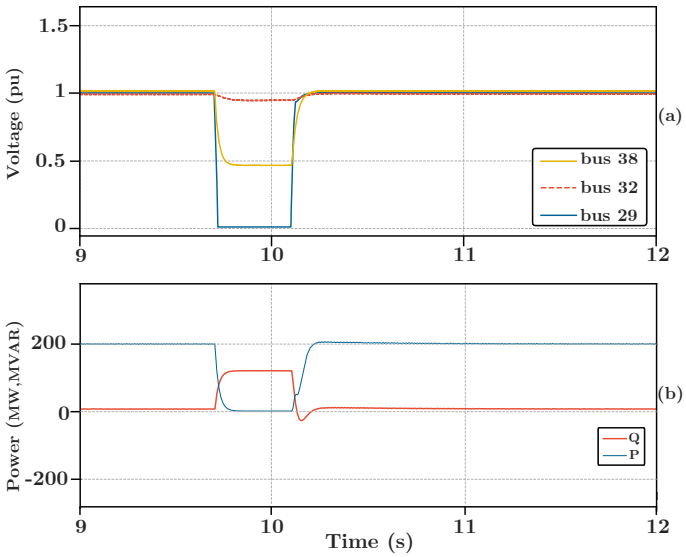

Fig. 5. Time-domain simulation results in the system with the optimized size and location of SynCons when FRT with the duration of 430 ms happens at bus 29 at t=9.7 s: (a) PoC voltages and (b) reactive and active power of the wind farm connected to bus 29.

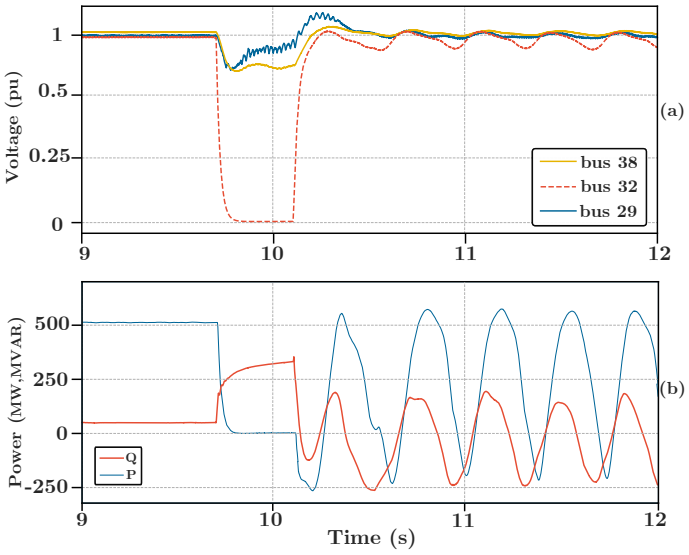

Fig. 6. Time-domain simulation results in the system with no SynCon installation when FRT with the duration of 430 ms happens at bus 32 at t=9.7 s: (a) PoC voltages and (b) reactive and active power of the wind farm connected to bus 32.

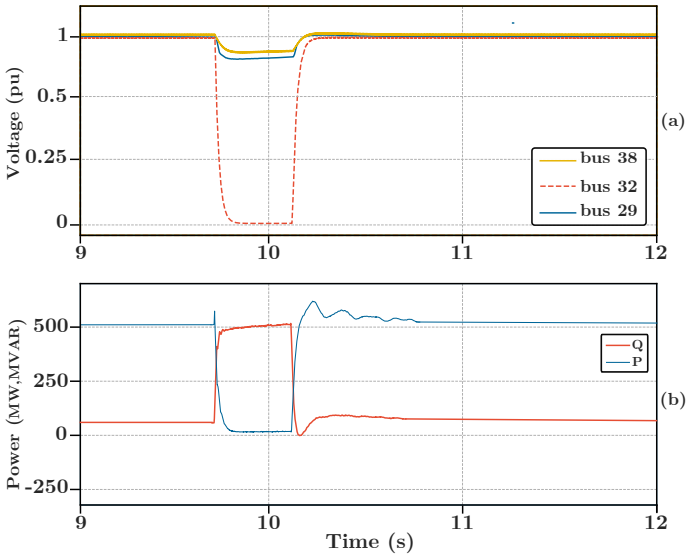

Fig. 7. Time-domain simulation results in the system with the optimized size and location of SynCons when FRT with the duration of 430 ms happens at bus 32 at t=9.7 s: (a) PoC voltages and (b) reactive and active power of the wind farm connected to bus 32.

and cleared after 430 ms. According to the NER [34], [37], RERs must ride through such a contingency.

- Multiple Fault Ride-Through (MFRT) Test: According to the NER, RERs should not trip through multiple disturbances in five minutes. . This test is applied at the PoCs to evaluate the performance of the optimized location and size of SynCons in a weak and low-inertia grid. Three three-phase faults with the duration of 430 ms are applied with four seconds difference between them at t=9.7 s, t=13.7 s, and t=17.7 s, respectively.

1) FRT Test at Bus 29: In this scenario, the FRT test is applied at bus 29 in the system with no SynCons and optimally sized and placed SynCons. The system is stable before the test, and the RERs work with their nameplate values. The wind farms at buses 29 and 32 generate 200 and 500 MW, respectively, and the solar farm at bus 38 supplies 200 MW.

FRT with no SynCon: Fig. 4(a) illustrates the PoC voltages before and after the FRT test for the wind farm connected at bus 29. The PoC voltages are stable before FRT test. However, after the FRT test clearance, a sustained 12 Hz oscillation is introduced on the buses 29 and 38 voltages. The magnitude

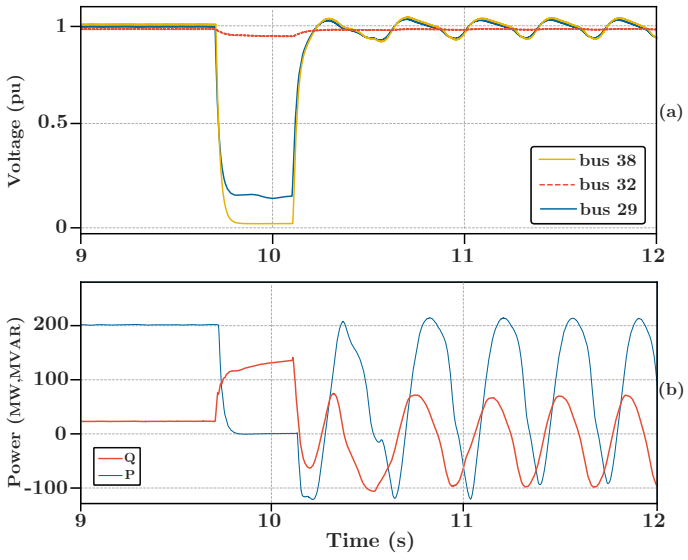

Fig. 8. Time-domain simulation results in the system with no SynCon installation when FRT with the duration of 430 ms happens at bus 38 at t=9.7 s: (a) PoC voltages and (b) reactive and active power of the wind farm connected to bus 38.

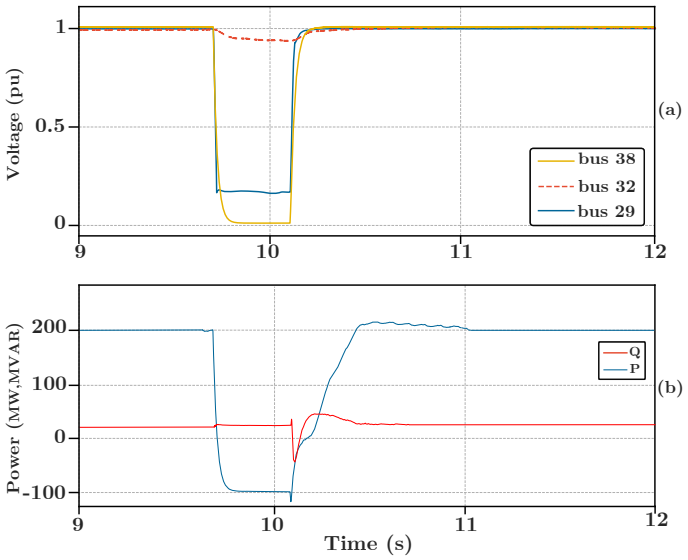

Fig. 9. Time-domain simulation results in the system with the optimized size and location of SynCons when FRT with the duration of 430 ms happens at bus 38 at t=9.7 s: (a) PoC voltages and (b) reactive and active power of the wind farm connected to bus 38.

of oscillation at bus 29 is noticeable and is around 0.5 pu. Fig. 4(b) shows the output power of the wind farm connected to bus 29. It injects 200 MW (1 pu) before the fault and regulates the voltage before and during the fault. However, after the test clearance, the reactive and active powers cannot reach their steady-state values and oscillate. Consequently, without SynCons installation, the wind farm installed at bus 29 does not have FRT capability.

FRT Test with Optimized SynCons: The PoC voltages are depicted in Fig. 5(a). The voltages are stable before and after the fault. Additionally, Fig. 5(b) shows the reactive and active power of the wind farm installed at bus 29. It injects 200 M efore and after the fault, and the system is stable after the test clearance. Therefore, the wind farm has FRT capability.

2) FRT Test at Bus 32: In this scenario, the FRT test happens at bus 32 in the system with no SynCons and optimally sized and placed SynCons. As a result, the system is stable before the test, and the RERs work with their nameplate values. The wind farms at buses 29 and 32 generate 200 and 500 MW, respectively, and the solar farm at bus 38 supplies 200 MW.

FRT with no SynCon: As depicted in Fig. 6(a), the PoC voltages are stable before the FRT test. Nevertheless, when the fault is removed, a 3 Hz oscillation is introduced by RERs on the PoC voltages. Also, Fig. 6(b) shows the wind farm integrated at bus 32 output power. Before the FRT test, the wind farm supplies 500 MW (1 pu) and regulates the voltage by injecting reactive power before and during the fault. However, after the fault is removed, both the reactive and active powers oscillate at 3 Hz. The magnitude of the active power oscillation is around 750 MW peak to peak, which is noticeable. Therefore, the wind farm installed bus 32 without the installation of SynCons does not have FRT capability.

FRT Test with Optimized SynCons: In this case, the FRT test happens at bus 32. Fig. 7(a) shows the PoC voltages in the system. All PoC voltages are stable before and after the fault. The voltages recover after the fault is removed less than 1 s. Moreover, Fig. 7(b) illustrates the reactive and active power output of the wind farm installed at bus 32. The wind farm supplies 500 MW (reactive power reaches the steady-state value) without any oscillation after the fault is removed, and the system is stable. In addition, the wind farm contributes with the reactive power during the fault. Therefore, with the optimized SynCons, the wind farm has FRT capability.

3) FRT Test at Bus 38: In this scenario, the FRT test is applied at bus 38 in the system with no SynCons and optimally sized and placed SynCons. As shown in Fig. 8 and Fig. 9 the system is stable before the test, and all voltages are between 0.95 pu and 1 pu. The RERs supply their nominal power to the system.

FRT with no SynCon: Fig. 8(a) illustrates the PoCs voltages prior, during, and after the FRT test. As shown in Fig. 8(a), the system is stable before the fault, and all PoC voltages are between 0.95 pu and 1 pu. However, after the fault is removed, bus 29 and bus 38 voltages oscillate with 3 Hz frequency. Moreover, as illustrated in Fig. 8(b), the solar farm at bus 38 injects its nameplate power (200 MW). Additionally, the solar farm injects reactive power to regulate the PoC voltage before and during the fault. Nevertheless, after the fault is removed, the reactive and active powers are not stable, and they cannot reach steady-state values. Consequently, the solar farm at bus 38 does not have FRT capability.

FRT Test with Optimized SynCons: As shown in Fig. 9(a), the voltages for all PoCs are stable before and after the fault. The voltages recover in less than 0.2 s after the fault is removed. There is no oscillation in the system. Also, Fig. 9(b) illustrates the output power of the solar farm connected at bus 38. The solar farm supplies 200 MW before and after the

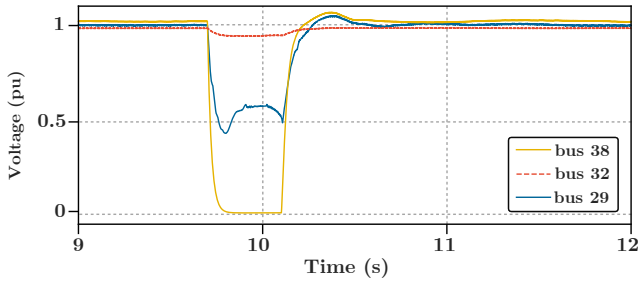

Fig. 10. PoC voltages when FRT with the duration of 430 ms is applied at bus 38 in the test-bed system with the optimized SynCons obtained by meta-heuristic optimization at t=9.7 s.

test. There is no oscillation in the reactive and active power output. Therefore, the solar farm has FRT capability.

The FRT test is applied at bus 38 in the system with optimized SynCons based on the heuristic algorithm proposed in [18] to compare the results achieved by the proposed convex optimization. The PoC voltages of the FRT test on bus 38 are illustrated in Fig. 10 . As shown in Fig. 9(a) and Fig. 10, with both convex and meta-heuristic algorithms, FRT capability is achieved. However, with the convex optimization, the total size of the installed SynCons is less than the total size obtained with the meta-heuristic one, which means a lower cost.

4) MFRT Test: In this case study, the MFRT test happens at all PoCs in the system with optimally sized and placed SynCons. Figs. 11(a) and 11(b) show the PoC voltages before, during, and after the MFRT test happens at buses 29, 32, and 38, respectively. As depicted in Fig. 11, the voltages are stable after each fault is removed. The voltages reach pre-fault steady-state situations in less than 0.5 s after the fault is removed. Therefore, the optimized results for the sizing and allocation of the SynCons add the MFRT capability to the RERs installed in the system.

5) FRT Test with Random Sizing and Allocation: In this scenario, the SynCons are utilized in the system with random locations or random sizes. In the case of random locations, optimal sizes listed in Table I are used. In the random size case, the SynCons are installed at the optimal locations based on Table I.

FRT Test with Random Allocation: In this case, the SynCons with the optimal sizes are located at buses 32, 10, 17, and 26. The FRT test is applied at bus 29. As shown in Fig. 12, the voltages at buses 29 and 38 have a sustained oscillation after the test clearance. The magnitude of the oscillation is lower than that in Fig. 4(a) in which no SynCon is installed in the system. However, the emergence of sub-synchronous oscillation is not acceptable.

FRT Test with Random Sizing: In this test, the FRT test is applied at bus 38 while the SynCons are located at optimal locations. The SynCon at bus 10 is selected larger than the optimal value (23 MVA), and the size of the SynCon at bus 29 is less than the optimal value (5 MVA). However, the total size of the SynCons is equal to the optimal value. As illustrated in Fig. 13, the PoC voltages have sub-synchronous oscillation after the FRT test. 3 Hz oscillation emerges on buses 29 and 38 voltage waveforms. Therefore, with the random sizing and

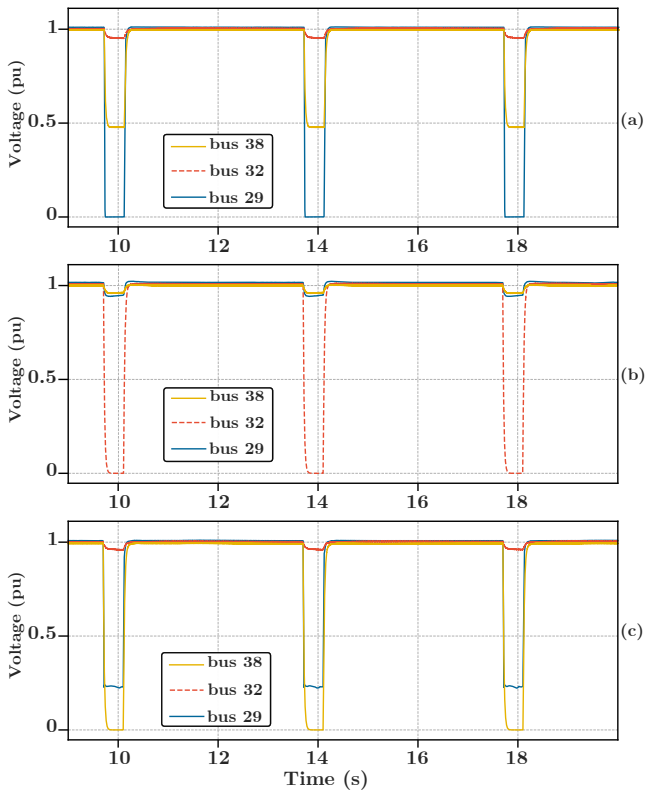

Fig. 11. Time-domain simulation results in the system with the optimized SynCons when MFRT test with a duration of 430 happens at the bus 29, bus 32, and bus 38 at t=9.7 s, t=13.7 s, and t=17.7 s: (a) PoC voltages when the MFRT happens at bus 29, (b) PoC voltages when MFRT happens at bus 32, and (c) PoC voltages when the MFRT happens at bus 38.

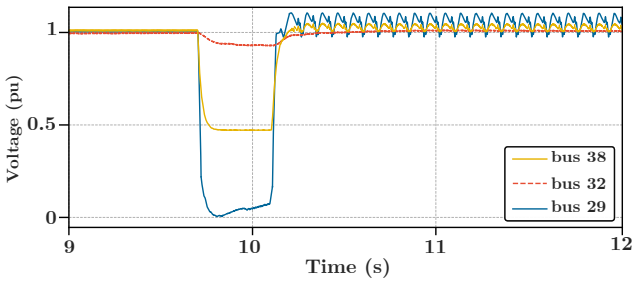

Fig. 12. Time-domain simulation results of PoC voltages in the system with random allocation of SynCons when FRT with the duration of 430 ms happens at bus 29 at t=9.7 s.

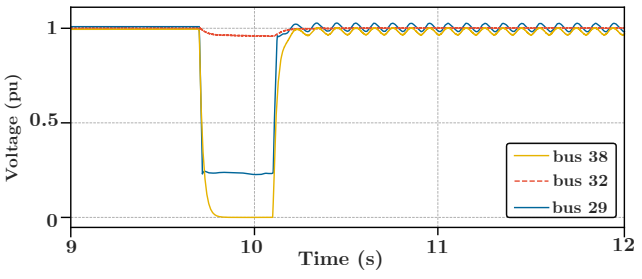

Fig. 13. Time-domain simulation results of PoC voltages in the system with random sizing of SynCons when FRT test with the duration of 430 ms happens at bus 38 at t=9.7 s.

TABLE III
POC VOLTAGES STDEV AND MSE VALUES FOR POST FRT TESTS

Test	Signal	Scenario							
		without SynCons		with optimized SynCons		with random allocation		with random sizing	
		MSE	stdev	MSE	stdev	MSE	stdev	MSE	stdev
FRT Test on bus 29	bus 29 Voltage	0.134913	0.13672	2.0497e-07	4.5256e-04	0.13408	0.1353	-	-
	bus 32 Voltage	0.000335	0.01431	5.6236e-06	18.0031e-06	0.00034	0.0121	-	-
	bus 38 Voltage	0.018805	0.05401	2.3445e-06	9.7552e-04	0.01730	0.0539	-	-
FRT Test on bus 32	bus 29 Voltage	0.001113	0.03220	1.4632e-07	3.6353e-04	-	-	-	-
	bus 32 Voltage	0.001504	0.03269	1.1579e-06	9.4566e-04	-	-	-	-
	bus 38 Voltage	0.001708	0.01298	2.0928e-06	9.5534e-04	-	-	-	-
FRT Test on bus 38	bus 29 Voltage	0.000918	0.02964	4.6968e-07	5.8680e-04	-	-	0.000561	0.02213
	bus 32 Voltage	2.062e-05	0.00416	5.8204e-04	0.0023	-	-	0.000031	0.00108
	bus 38 Voltage	0.001420	0.03490	2.0198e-06	0.0012	-	-	0.000853	0.02726

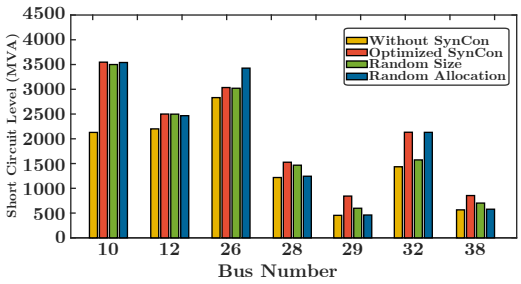

Fig. 14. Short circuit level of PoCs and their nearby buses in different scenarios of SynCons operation.

allocation of the SynCons, the RERs in the system do not have the FRT capability, although the total installation size is equal to the total optimal size. Fig. 14 shows the short circuit level of the PoCs (buses 29, 32, and 38) together with certain nearby buses, in four different scenarios: 1) the system without SynCons, 2) the system with optimized SynCons, 3) the system with SynCons with reduced size, and 4) the system with SynCons with random allocation. RERs size installed at buses 29, 32, and 38 is 200, 500, and 200 MVA, respectively. Therefore, for having an SCR greater than three, the short circuit level at buses 29, 32, and 38 must be greater than 600, 1500, and 600 MVA, respectively. As shown in Fig. 14, with the random allocation of SynCons or with the reduced optimized size of SynCons, buses 29 and 38 have a short circuit level of less than 600 MVA, which based on the size of RERs connected to these buses, the SCR is less than three.

Moreover, to analyze the performance of the results of the proposed optimization method, the standard deviation (stdev) and Mean Square Error (MSE) are utilized as described in [18]. Table III shows the MSE and stdev indices of buses 29, 32, and 38 voltage waveforms in different FRT tests. The indices are lower when the optimal number, place, and size of SynCons are utilized compared to the random sizing and random allocation of SynCons. In addition, the stdev and MSE indices with the proposed convex optimization are lower than or equal to the indices obtained by meta-heuristic methods [18].

IV. CONCLUSIONS

This paper proposes a mixed-integer convex optimization formulation to find the optimal number, location, and size of SynCons in weak and low-inertia grid integration of RERs, while the SCR for all PoCs is maintained above given values and the cost of the SynCons utilization is minimized. The key to this formulation is the observation that the SCR constraint can be expressed in a convex form. This formulation allows the problem to be solved to global optimality. Therefore, global optimality can be guaranteed. The proposed optimization method is applied to the IEEE 39-bus system, and the system is modeled in detail in PSCAD/EMTDC. The optimization procedure is fast and easy to apply in different systems. The simulation results show that the system with the optimal installation of SynCons compared to the system with no SynCons or with non-optimal SynCons is stable, and all RERs in the system can earn the FRT and MFRT capability. Therefore, the proposed optimization method paves the way for the deployment of SynCons in the power systems and minimizes their cost drawback.

ACKNOWLEDGMENT

This work has been supported by the Monash Grid Innovation Hub and the Australian Renewable Energy Agency (ARENA) under the Advancing Renewable Program (Grant No.: 2020/ARP007).

REFERENCES

[1] H. Gu, R. Yan, and T. K. Saha, "Minimum synchronous inertia requirement of renewable power systems," *IEEE Trans. Power Syst.*, vol. 33, no. 2, pp. 1533–1543, March 2018.

[2] C. Phurailatpam, Z. H. Rather, B. Bahrani, and S. Doolla, "Measurement-based estimation of inertia in ac microgrids," *IEEE Trans. Sustain. Energy*, vol. 11, no. 3, pp. 1975–1984, July. 2020.

[3] C. Phurailatpam, Z. H. Rather, B. Bahrani, and S. Doolla, "Estimation of non-synchronous inertia in ac microgrids," *IEEE Trans. Sustain. Energy*, April. 2021, Early Access.

[4] S. Lu, Z. Xu, L. Xiao, W. Jiang, and X. Bie, "Evaluation and enhancement of control strategies for vsc stations under weak grid strengths," *IEEE Trans. Power Syst.*, vol. 33, no. 2, pp. 1836–1847, March 2018.

[5] D. Wang, L. Liang, L. Shi, J. Hu, and Y. Hou, "Analysis of modal resonance between pll and dc-link voltage control in weak-grid tied vscs," *IEEE Trans. Power Syst.*, vol. 34, no. 2, pp. 1127–1138, March 2019.

[6] M. Zhao, X. Yuan, J. Hu, and Y. Yan, "Voltage dynamics of current control time-scale in a vsc-connected weak grid," *IEEE Trans. Power Syst.*, vol. 31, no. 4, pp. 2925–2937, July 2016.

[7] W. G. B4.62, "Connection of wind farms to weak ac networks," in *Cigre Technical Brochure 671*. CIGRE, December 2016.

[8] W. Du, Q. Fu, and H. Wang, "Subsynchronous oscillations caused by open-loop modal coupling between vsc-based hvdc line and power system," *IEEE Trans. Power Syst.*, vol. 33, no. 4, pp. 3664–3677, July 2018.

[9] H. Liu, X. Xie, and W. Liu, "An Oscillatory Stability Criterion Based on the Unified *dq*-Frame Impedance Network Model for Power Systems With High-Penetration Renewables," *IEEE Trans. Power Syst.*, vol. 33, no. 3, pp. 3472–3485, May 2018.

[10] Y. Xu, Z. Gu, and K. Sun, "Characterization of subsynchronous oscillation with wind farms using describing function and generalized nyquist criterion," *IEEE Trans. Power Syst.*, vol. 35, no. 4, pp. 2783–2793, July 2020.

[11] H. Liu and X. Xie, "Comparative studies on the impedance models of vsc-based renewable generators for ssi stability analysis," *IEEE Trans. Energy Convers.*, vol. 34, no. 3, pp. 1442–1453, Sept. 2019.

[12] V. Jain and B. Singh, "A multiple improved notch filter-based control for a single-stage pv system tied to a weak grid," *IEEE Trans. Sustain. Energy*, vol. 10, no. 1, pp. 238–247, 2019.

[13] J. Liu, W. Yao, J. Wen, J. Fang, L. Jiang, H. He, and S. Cheng, "Impact of power grid strength and pll parameters on stability of grid-connected dfig wind farm," *IEEE Trans. Sustain. Energy*, vol. 11, no. 1, pp. 545–557, Jan. 2020.

[14] C. Yang, L. Huang, H. Xin, and P. Ju, "Placing grid-forming converters to enhance small signal stability of pll-integrated power systems," *IEEE Trans. Power Syst.*, Dec. 2020, Early Access.

[15] L. Fan and Z. Miao, "An explanation of oscillations due to wind power plants weak grid interconnection," *IEEE Trans. Sustain. Energy*, vol. 9, no. 1, pp. 488–490, 2018.

[16] D. B. Rathnayake, M. Akrami, C. Phurailatpam, S. P. Me, S. Hadavi, G. Jayasinghe, S. Zabihi, and B. Bahrani, "Grid forming inverter modeling, control, and applications," *IEEE Access*, vol. 9, pp. 114 781–114 807, 2021.

[17] H. T. Nguyen, G. Yang, A. H. Nielsen, and P. H. Jensen, "Combination of synchronous condenser and synthetic inertia for frequency stability enhancement in low-inertia systems," *IEEE Trans. Sustain. Energy*, vol. 10, no. 3, pp. 997–1005, July 2019.

[18] S. Hadavi, M. Z. Mansour, and B. Bahrani, "Optimal allocation and sizing of synchronous condensers in weak grids with increased penetration of wind and solar farms," *IEEE Journal on Emerging and Selected Topics in Circuits and Systems*, vol. 11, no. 1, pp. 199–209, Jan. 2021.

[19] L. Wang, Q. Jiang *et al.*, "Impact of synchronous condenser on sub/super-synchronous oscillations in wind farms," *IEEE Trans. Power Del.*, Aug. 2020, Early Access.

[20] A. Moeini and I. Kamwa, "Analytical concepts for reactive power based primary frequency control in power systems," *IEEE Trans. Power Syst.*, vol. 31, no. 6, pp. 4217–4230, Jan. 2016.

[21] S. Hadavi, D. Rathnayake, S. G. Jayasinghe, A. Mehrizi-Sani, and B. Bahrani, "A robust exciter controller design for synchronous condensers in weak grids," *IEEE Trans. Power Syst.*, Sept. 2021.

[22] J. Jia, G. Yang, A. H. Nielsen, and V. Gevorgian, "Investigation on the combined effect of vsc-based sources and synchronous condensers under grid unbalanced faults," *IEEE Trans. Power Del.*, vol. 34, no. 5, pp. 1898–1908, May 2019.

[23] H. T. Nguyen, G. Yang, A. H. Nielsen, and P. H. Jensen, "Hardware- and software-in-the-loop simulation for parameterizing the model and control of synchronous condensers," *IEEE Trans. Sustain. Energy*, vol. 10, no. 3, pp. 1593–1602, 2019.

[24] F. O. Igbinovia, G. Fandi, Z. Müller, J. Švec, and J. Tlustỳ, "Optimal location of the synchronous condenser in electric-power system networks," in *17th International Scientific Conference on Electric Power Engineering (EPE)*, 2016.

[25] N.-A. Masood, R. Yan, T. K. Saha, and S. Bartlett, "Post-retirement utilisation of synchronous generators to enhance security performances in a wind dominated power system," *IET Generation, Transmission & Distribution*, vol. 10, no. 13, pp. 3314–3321, June 2016.

[26] Z. H. Rather, Z. Chen, P. Thøgersen, and P. Lund, "Dynamic reactive power compensation of large-scale wind integrated power system," *IEEE Trans. on Power Syst.*, vol. 30, no. 5, pp. 2516–2526, Sept. 2014.

[27] J. Jia, G. Yang, A. H. Nielsen, E. Muljadi, P. Weinreich-Jensen, and V. Gevorgian, "Synchronous condenser allocation for improving system short circuit ratio," in *2018 5th International Conference on Electric Power and Energy Conversion Systems (EPECS)*. IEEE, 2018.

[28] L. Richard, Nahid-Al-Masood, T. K. Saha, W. Tushar, and H. Gu, "Optimal allocation of synchronous condensers in wind dominated power grids," *IEEE Access*, vol. 8, pp. 45 400–45 410, March 2020.

[29] E. Marrazi, G. Yang, and P. Weinreich-Jensen, "Allocation of synchronous condensers for restoration of system short-circuit power," *Journal of Modern Power Systems and Clean Energy*, vol. 6, no. 1, pp. 17–26, 2018.

[30] A. M. Kettner and M. Paolone, "On The Properties of The Power Systems Nodal Admittance Matrix," *IEEE Transactions on Power Systems*, vol. 33, no. 1, pp. 1130–1131, 2017.

[31] D. Turizo and D. K. Molzahn, "Invertibility Conditions for the Admittance Matrices of Balanced Power Systems," *arXiv preprint arXiv:2012.04087*, 2020.

[32] P. F. Curran, "On a variation of the gershgorin circle theorem with applications to stability theory," 2009.

[33] MOSEK ApS., *The MOSEK Optimization Toolbox for MATLAB Manual v9.2.29*, Accessed:Aug. 12, 2020. [Online]. Available: https://docs.mosek.com/9.2/toolbox.pdf

[34] AMEC, "National Electricity Rules version 160," 2020.

[35] J. Löfberg, "YALMIP :a toolbox for modeling and optimization in MATLAB," in *IEEE Int. Conf. on Robotics and Automation (IEEE Cat. No.04CH37508)*, 2004, pp. 284–289.

[36] K. Máslo, A. Kasembe, and M. Kolcun, "Simplification and Unification of IEEE Standard Models for Excitation Systems," *Electric Power Systems Research*, vol. 140, pp. 132–138, 2016.

[37] M. Mohseni and S. M. Islam, "Transient control of DFIG-based wind power plants in compliance with the Australian grid code," *IEEE Trans. Power Electron.*, vol. 27, no. 6, pp. 2813–2824, 2011.

[38] F. Zhang, *The Schur complement and its applications*. Springer Science & Business Media, 2006, vol. 4.

APPENDIX A
LMI REFORMULATION OF THE SCR CONSTRAINT

The reformulation of (10) as (12b) and (12c), is based on the following result.

Lemma 1. *Let L be a fixed positive definite matrix. Then,*

$$\begin{aligned}\{H : H \succeq 0,\ [L+H]_{ii}^{-1} \le b_i\ \forall i\} \\ = \{H : \exists T \ \ s.t.\ H \succeq 0, \\ \begin{bmatrix} T & I \\ I & L+H \end{bmatrix} \succeq 0\ ,\ T_{ii} \le b_i\ \forall i\}. \end{aligned} \quad (14)$$

Proof. The justification of this fact involves showing that an arbitrary element on the left-hand side is also an element on the right-hand side (LHS $\subseteq$ RHS) and that an arbitrary element on the right-hand side is also an element on the left-hand side (RHS $\subseteq$ LHS).

(LHS $\subseteq$ RHS): Let H be an element of the left hand side of (14), i.e., $H \succeq 0$ and satisfies $[L+H]_{ii}^{-1} \le b_i$ for $i \in V$. Let $T = (L+H)^{-1}$. Then $T_{ii} \le b_i$ for $i \in V$. Since L is strictly positive definite, and H is positive semi-definite, $L+H$ is strictly positive definite. Therefore, by the Schur complement lemma (see, e.g., [38, Theorem 1.12(b)]),

$$\begin{bmatrix} T & I \\ I & L+H \end{bmatrix} \succeq 0 \quad \iff \quad T - (L+H)^{-1} \succeq 0.$$

Since $T = (L+H)^{-1}$, it follows that $T-(L+H)^{-1} = 0 \succeq 0$, and so that

$$\begin{bmatrix} T & I \\ I & L+H \end{bmatrix} \succeq 0.$$

This establishes that H is an element of the right-hand side of (14).

(RHS $\subseteq$ LHS): Suppose that H is an element of the right hand side of (14), i.e., $H \succeq 0$ and there exists a T such that $T_{ii} \le b_i$ for $i \in V$ and $\left[\begin{smallmatrix} T & I \\ I & L+H \end{smallmatrix}\right] \succeq 0$. Then, since $L+H$ is positive definite, by the Schur complement lemma, $T-(L+H)^{-1} \succeq 0$. Since the diagonal entries of positive semi-definite matrices are nonnegative, it follows that $[L+H]_{ii}^{-1} \le T_{ii} \le b_i$ for $i \in V$. Thus, H is an element of the left-hand side of (14), completing the argument. □

The reformulation of (10) as (12b) and (12c) follows by applying Lemma 1 with $L = W_{\text{bus}}$ and $H = \text{diag}(W)$. The assumptions of Lemma 1 are satisfied, and it can be applied in this case because W_{bus} is strictly positive definite, and because the constraint (12e) implies that $W_i \geq 0$ for all $i \in V$.

Sajjad Hadavi (S'19) received the B.Sc. and M.Sc. degrees in electrical engineering from Amirkabir University of Technology, Tehran, Iran, in 2013 and 2015, respectively. Since 2018 he has been pursuing a Ph.D. degree at Monash University, Australia. His research interests include control of power electronics systems, power electronics in power systems, and grid integration of renewable energy resources.

James Saunderson (M'16) received the B.Sc. degree in mathematics and the B.E. degree in electrical and electronic engineering from the University of Melbourne, Australia, both in 2008. He received the S.M. and the Ph.D. degrees in Electrical Engineering and Computer Science from Massachusetts Institute of Technology in 2011 and 2015, respectively.

From June 2015–July 2016 he was a Postdoctoral Scholar at Caltech and at the University of Washington, Seattle, both in Electrical Engineering. Since July 2016 he has been a Lecturer in Electrical and Computer Systems Engineering at Monash University, in Melbourne, Australia. His research focuses on mathematical optimization and its applications.

Dr Saunderson was the recipient of the 2020 SIAM Activity Group on Optimization Best Paper Prize, and a 2021 Australian Research Council Discovery Early Career Researcher Award. He is currently an associate editor of the SIAM Journal on Applied Algebra and Geometry.

Ali Mehrizi-Sani (S'05–GS'08–M'12–SM'15) received the B.Sc. degrees in electrical engineering and petroleum engineering from Sharif University of Technology, Tehran, Iran, both in 2005. He received the M.Sc. degree from the University of Manitoba, Winnipeg, MB, Canada, and the Ph.D. degree from the University of Toronto, Toronto, ON, Canada, both in electrical engineering, in 2007 and 2011. He is currently an Associate Professor at Virginia Tech, Blacksburg, VA, USA. His areas of interest include power system applications of power electronics and integration of renewable energy resources. Dr. Mehrizi-Sani is an editor of IEEE TRANSACTIONS ON ENERGY CONVERSION, IEEE POWER ENGINEERING LETTERS, MDPI Energies, and MDIP Electronics. He is the recipient of 2018 IEEE PES Outstanding Young Engineer Award, 2018 ASEE PNW Outstanding Teaching Award, 2017 IEEE Mac E. Van Valkenburg Early Career Teaching Award, 2017 WSU EECS Early Career Excellence in Research, 2016 WSU VCEA Reid Miller Excellence in Teaching Award, and 2007 Dennis Woodford prize for his M.Sc. thesis. From 2007 to 2011, he was a Connaught Scholar at the University of Toronto.

Behrooz Bahrani Behrooz Bahrani (M'13–SM'19) received the B.Sc. degree from Sharif University of Technology, Tehran, Iran, the M.Sc. degree from the University of Toronto, Toronto, ON, Canada, and the PhD degree from the Ecole Polytechnique Fédérale de Lausanne (EPFL), Lausanne, Switzerland, all in electrical engineering, in 2006, 2008, and 2012, respectively. From September 2012 to September 2015, he was a Postdoctoral Fellow at several institutions including EPFL, Purdue University, West Lafayette, IN, USA, Georgia Institute of Technology, Atlanta, GA, USA, and the Technical University of Munich, Munich, Germany. Since 2015, he has been with Monash University, Clayton, Australia, where currently, he is a Senior Lecturer and the Director of the Grid Innovation Hub. His research interests include control of power electronics systems, applications of power electronics in power and traction systems, and grid integration of renewable energy resources.